Titan's stratospheric composition driven by condensation and dynamics

Frédéric Hourdin and Sébastien Lebonnois
Laboratoire de Météorologie Dynamique, Institut Pierre-Simon Laplace, Paris, France

David Luz
LESIA, Observatory of Paris, Meudon, France and Centro de Astronomia e Astrofísica da Universidade de Lisboa, Lisbon, Portugal

Pascal Rannou
Service d'Aéronomie, Institut Pierre-Simon Laplace, Paris, France

Received 20 April 2004; revised 9 July 2004; accepted 18 August 2004; published 23 December 2004.

[1] Atmospheric transport of chemical compounds and organic haze in the stratosphere of Titan is investigated with an axisymmetric general circulation model. It has been shown previously that the meridional circulation, dominated by global Hadley cells, is responsible both for the creation of an intense stratospheric zonal flow and for the accumulation of chemical compounds and haze in high latitudes. The modified composition in turn intensifies the meridional circulation and equator-to-pole thermal contrasts. This paper analyzes in detail the transport processes responsible for the observed vertical and latitudinal variations of atmospheric composition. It is shown that the competition between rapid sinking of air from the upper stratosphere in the winter polar vortex and latitudinal mixing by barotropic planetary waves (parameterized in the model) controls the vertical gradient of chemical compounds. The magnitude of polar enrichment (of a factor 1.4 to 20 depending on the particular species) with respect to low latitudes is mostly controlled by the way the meridional advection increases the concentrations of chemical compounds in the clean air which is rising from the troposphere, where most of the chemical compounds are removed by condensation (the temperature at the tropopause being close to 70 K). The agreement between the observed and simulated contrasts provides an indirect but strong validation of the simulated dynamics, thus confirming the explanation put forward for atmospheric superrotation. It is shown also that by measuring the atmospheric composition, the Cassini-Huygens mission will provide a strong constraint about Titan's atmospheric circulation. *INDEX TERMS:* 5707 Planetology: Fluid Planets: Atmospheres—structure and dynamics; 5704 Planetology: Fluid Planets: Atmospheres—composition and chemistry; 6280 Planetology: Solar System Objects: Saturnian satellites;
KEYWORDS: composition, stratospheric dynamics, Titan

Citation: Hourdin, F., S. Lebonnois, D. Luz, and P. Rannou (2004), Titan's stratospheric composition driven by condensation and dynamics, *J. Geophys. Res.*, *109*, E12005, doi:10.1029/2004JE002282.

1. Introduction

[2] The atmosphere of Titan, which will be soon observed by the Cassini/Huygens mission, is one of the most mysterious and exciting climate systems of the solar system. Titan's dense nitrogen atmosphere (1.4 atm at the surface for a gravity of 1.35 m s^{-2}) is thought to be dominated by a strong zonal flow, peaking in the stratosphere at around 200–300 km. At these altitudes, the atmosphere is rotating about 10 times faster than the solid body, itself locked in phase around Saturn, with a 16-day period. Composed mainly of nitrogen (90–98%) and methane (2% above tropopause), Titan's atmosphere is also the site of an intense photochemistry, initiated between 600 and 1000 km by dissociation of molecules by magnetospheric electrons and UV photons. Laboratory experiments suggest that compounds as complex as "ammono" analogs to amino acids could be present [*Raulin and Owen*, 2002]. About 20 different species have been detected thus far, either by Voyager or from ground-based observations. This rich photochemistry yields polymerization of hydrocarbons and nitriles, with formation of a dense aerosol layer in the stratosphere, that gives Titan its orange color on Voyager visible images. The details of this polymerization are not yet understood, and both experimental and theoretical studies are in progress on this point [*Coll et al.*, 1999; *Tran et al.*, 2003; *Lebonnois et al.*, 2002; *Wilson and Atreya*, 2003].

0148-0227/04/2004JE002282$09.00

[3] Almost all the gaseous species show a strong enrichment in the northern polar latitudes at the time of Voyager encounter, shortly after northern spring equinox. If defined as the ratio between the average concentration at 50–70 N and that at 0–30 N, this enrichment varies from a factor of 1.4 to more than 20 depending on the particular chemical compound.

[4] In a review of the composition of Titan's atmosphere from a meteorological viewpoint, [*Flasar*, 1998] suggests that the meridional transport and subsidence of stratospheric species could play a significant role in enhancing the polar concentration. From meridional winds of 4 m s^{-1} and a dynamical time scale ~4 terrestrial years, he estimated an HCN enhancement of a factor of 2, and concluded that some additional factor, such as a localized meridional circulation, was necessary to explain the observations. He also discusses the possibility of the circumpolar vortex becoming dynamically and compositionally isolated from the remainder of the atmosphere during late winter and early spring. In a speculative analogy with Earth's ozone hole, the isolation would end with the breaking of the vortex by planetary waves, which would mix constituents, heat and vorticity across the boundary.

[5] Combining a photochemical model and transport of atmospheric compounds by meridional circulation, [*Lebonnois et al.*, 2001] have clearly attributed the enrichment of northern high latitudes at the time of Voyager to the downward advection of chemical compounds from the production zone, in the downward branch of a global pole-to-pole Hadley cell which prevails almost until northern spring equinox. Without additional factors, the coupled model was able to reproduce even the large value observed for the polar enrichment of HCN. No clear explanation was given however for the wide range observed for the magnitude of this polar enrichment. [*Lebonnois et al.*, 2001] suggested that this magnitude could be partly controlled by chemistry: a stronger contrast on the vertical, due for instance to a stronger source in the upper atmosphere relatively to the sinks, could produce, through downward advection in high latitudes, a stronger polar enrichment.

[6] The present paper casts a new light on this question. For most species, the magnitude of the latitudinal contrast does not depend in fact on the actual chemistry but only on the altitude at which they condense. We show that the very same latitudinal contrasts can be obtained either with a full chemical model forced by the GCM dynamics or with a very simple tracer fixed to one in the upper stratosphere and undergoing advection and condensation at a given level. It is shown also that advection in the meridional plane and latitudinal mixing by waves is controlling the vertical gradient of chemical compounds.

[7] If atmospheric transport is responsible for the latitudinal and vertical variations of the stratospheric composition, then observations of composition can also provide valuable information on the atmospheric circulation. In particular, the good agreement of model results and observations in terms of polar enrichment and vertical profiles provides a strong validation of the atmospheric dynamics given that this polar enrichment is quite sensitive to the model dynamics. In fact, polar enrichment in itself is evidence for the existence of the Hadley circulation on Titan. This fundamental component of the dynamics has never been directly observed on Titan. Observations of the latitudinal and time variations of atmospheric composition by the Cassini orbiter will thus contain very important constraints on the atmospheric circulation.

[8] The paper begins with a synthesis of previous modeling work on the simulation of the atmospheric composition and dynamics of Titan's atmosphere including a description of the version of the coupled model used in this study (section 2). We then discuss what controls the vertical and latitudinal variations of atmospheric chemical compounds (section 3) and how their simulation depends on the accuracy of the simulated atmospheric dynamics (section 4). Seasonal variations are discussed in section 5. We finally present some predictions of what Cassini should observe during the mission and underline the importance an extended mission covering a longer fraction of a Titan year could have (section 6) before some concluding remarks.

2. Titan Climate Modeling

2.1. Atmospheric Superrotation

[9] *Golitsyn* [1975] was the first to suggest that, like Venus, Titan may be the site of an intense atmospheric superrotation. Observations of latitudinal temperature contrasts by the Voyager 1 probe [*Flasar et al.*, 1981] as well as the shape of Titan's atmosphere (reconstructed from ground-based observations of the occultation of a very bright star [*Hubbard*, 1993]) both suggested a strong zonal flow, but with no constraint on its direction.

[10] The prograde nature of winds was first predicted theoretically and simulated numerically with a general circulation model adapted from the climate model of the Laboratoire de Météorologie Dynamique [*Hourdin et al.*, 1992, 1995], LMDZ. It has since gained mounting observational confirmation [*Kostiuk et al.*, 2001; *Moreno and Marten*, 2003; *Bouchez et al.*, 2003b; *Luz et al.*, 2003a].

[11] The adaptation of the climate model from Earth to Titan mainly consisted in turning off the water cycle and replacing the radiative transfer computation by the code developed for Titan by *Toon et al.* [1989] for the solar range (UV and IR) and *McKay et al.* [1989] for the thermal IR. In this first study [*Hourdin et al.*, 1995], the radiative effect of latitudinal variations of the atmospheric composition was ignored. The three-dimensional dynamical core, based on the primitive equations of meteorology, was kept unchanged except for parameters such as gravity or the thermodynamic gas constant. Those simulations have been preceded by simpler studies [*Hourdin et al.*, 1992; *Del Genio et al.*, 1993; *Hourdin et al.*, 1996] for idealized planetary conditions in which superrotation has been obtained for planets rotating much slower than the Earth, at zero obliquity (as on Venus) and increased absorption of solar radiation in the visible.

[12] Both for the realistic Titan case and for the simpler simulations mentioned above, the simulated superrotation is explained by the so-called Gierasch-Rossow mechanism [*Gierasch*, 1975]. The net upward transport of angular momentum (product of the absolute zonal velocity and the distance to the polar axis) by global equator-to-pole Hadley cells is able to create and maintain an excess of angular momentum in the upper atmospheric layers, if the angular momentum is larger in low than in high latitudes (this is the case for instance for an atmosphere at rest with respect to

the surface). Once superrotation sets in, there is also more angular momentum transported into high latitudes in the upper branches of the Hadley cells than equatorward near the surface. This net poleward transport of angular momentum is balanced by equatorward transport by nonaxisymmetric eddies as originally suggested by *Gierasch* [1975] and *Rossow* [1979] in the context of Venus. In the numerical simulations, those eddies were identified as planetary waves forced by barotropic and inertial instabilities on the equatorward flank of the strong high-latitude jets created, like the jet stream on Earth, by the poleward transport of angular momentum from the equator. In this context, the slow planetary rotation rate is important to allow the Hadley circulation to extend up to the pole [*Hunt*, 1979; *Del Genio and Suozzo*, 1987] while the increased static stability reduces the coupling between the surface and the superrotating atmosphere.

[13] The main difference between Titan simulations [*Hourdin et al.*, 1995] and the above mentioned simulations of atmospheric superrotation is the strong seasonal cycle arising from Titan's large obliquity (26.7°): during almost half a year around solstice, the meridional circulation is dominated by a Hadley cell extending between both poles, with rising motion in the summer hemisphere. This meridional circulation creates an intense circumpolar jet in the winter hemisphere, analogous to the jet stream on Earth. It is only close to the equinoxes or on an annually averaged view that the meridional circulation is dominated by two equator-to-pole Hadley cells.

[14] For more details see the introduction of *Luz and Hourdin* [2003].

2.2. Coupling With Atmospheric Composition

[15] Those first simulations of Titan's atmospheric circulation strongly underestimated the latitudinal temperature contrasts measured by Voyager in the stratosphere as well as the intensity of the circumpolar jet inferred from the stellar occultation. [*Hourdin et al.*, 1995] suggested that this deficiency could be due to the fact that the radiative computations did not take into account the latitudinal contrasts in atmospheric composition or haze opacity.

[16] Modeling work and analysis of Voyager observations did confirm the strong coupling between chemistry, microphysics and stratospheric dynamics. By forcing a microphysical model of Titan's haze by the meridional circulation predicted with the Titan's GCM, it was shown that meridional transport alone could explain the order of magnitude of the observed hemispheric and seasonal contrasts in Titan's albedo [*Hutzell et al.*, 1995]. With a similar approach, the polar enrichment in gaseous compounds at the time of the Voyager encounter was attributed to downward advection from source regions in the subsiding branch of the Hadley cell [*Lebonnois et al.*, 2001]. Finally, from radiative computations, it was shown that the latitudinal variations of atmospheric composition and haze opacity, as deduced from Voyager observations, were able to modulate significantly the radiative balance of Titan's stratosphere [*Bézard et al.*, 1995].

2.3. Two-Dimensional Coupled Model

[17] For the reasons above, it was then decided to develop a climate model for Titan, coupling dynamics, chemistry and haze microphysics. Because of the prohibitive numerical cost of the three-dimensional Titan GCM, the model was developed on the basis of a restriction to the axisymmetric component. The microphysical model by *Cabane et al.* [1992] was introduced in the climate model based on a description of the haze particles in terms of 10 bins in radius (instead of the 45 bins of the original one-dimensional model). The smallest size is for the freshly created macromolecules ($r_1 = 1.64 \times 10^{-9}$ m), the other radii being given by $r_{n+1} = 16^{1/3} r_n$. The monomer radius is $r_m = 66$ nm and the volume ratio between two adjacent bins is 16. Particles larger than r_m are represented as fractal aggregates. The radiative code was upgraded to account for the coupling with the new aerosol description [*Rannou et al.*, 2004]. The atmospheric composition is handled by a module consisting essentially of the photochemical model of *Lebonnois et al.* [2001], which has been integrated in the GCM. This yields a stratospheric composition in rather good agreement with available observations, as shown in Figure 1. A detailed analysis of the most significant discrepancies (C_2H_6, C_3H_8, C_4H_2, HC_3N), and comparison with the previous results of *Lebonnois et al.* [2001] is not in the scope of this paper, and will be published in a forthcoming study. As done by *Lebonnois et al.* [2001], linear tracers can also be used for C_2H_6, C_2H_2 and HCN (thereafter named linearized chemistry). The chemical production and loss terms are replaced by relaxation toward a reference profile with a given photochemical time constant, both taken from a one-dimensional photochemical model. The advantages of this simplified chemistry are twofold: 1) the code is faster and 2) the model can be tuned so as to reproduce the observed mean stratospheric concentrations. This is important when evaluating the effect of chemical composition on atmospheric dynamics. Latitudinal profiles obtained with the linearized chemistry for these three compounds are also shown in Figure 1. In the present study, both the full and linearized chemistry are used.

[18] When using the full chemistry, the upper boundary has to be chosen for all species. Chemistry taking place above the GCM limits has a crucial role for most constituents, which are produced in the mesosphere and then transported downward. For the simulations used in this paper, we decided to fix the exchange flux between the upper atmosphere and the upper layer of the GCM. These fluxes are calculated using a one-dimensional model of Titan's atmosphere in equatorial conditions [see *Lebonnois et al.*, 2002, 2003a]. As a first approximation, these fluxes are fixed, both in time and as a function of latitude. A second option is to fix the composition in the upper layer of the GCM. This option was also tested, again with no temporal or latitudinal variations, and it gives results very similar to our first option. For the linearized chemistry, the upper boundary condition is handled in a different way: the concentration is forced to stay close to the one-dimensional reference profile in the three upper layers by imposing arbitrarily short chemical time constants (1 Titan day in the top layer, 10 days in the second and 100 days in the third layer from the top). The upper condition essentially controls the mean stratospheric concentration without affecting latitudinal contrasts, as will be shown below.

[19] To avoid difficulties related to the possible impact of temperature errors, condensation is computed for each

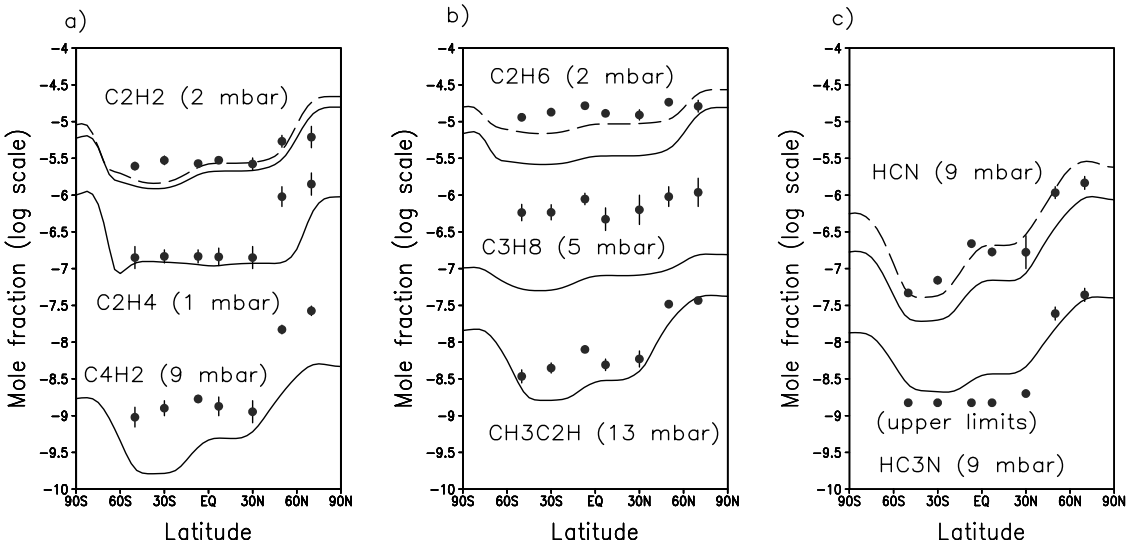

Figure 1. Comparison between simulated and observed stratospheric composition at solar longitude L_s = 9 (Voyager 1 flyby). Model results including full chemistry are plotted with solid lines. Dashed lines are for the linearized chemistry (see text). Black circles are observations from Voyager 1 [*Coustenis and Bézard*, 1995]. Pressure levels correspond to the maximum of the contribution function (at equator) for each compound. For the model, concentrations are extracted at this particular pressure level. Observations for HC_3N at low to mid latitudes are upper limits.

species (both for the full and linearized chemistry) from a concentration at saturation estimated once at the beginning of the simulation using the temperature profile of *Lellouch et al.* [1989].

[20] One important point when reducing the model to a two-dimensional latitude-altitude version, is to parameterize the effect of latitudinal transport of momentum, heat, or tracers by planetary waves. For this, a specific parameterization was developed [*Luz et al.*, 2003b]. In this parameterization, latitudinal mixing by waves is prescribed as an eddy diffusion. The eddy diffusivity K_y itself is parameterized as a function of the explicit variables of the axisymmetric model (closure). This parameterization was developed and tuned on the basis of a series of simulations of planetary waves in Titan-like conditions with a global shallow water model [*Luz and Hourdin*, 2003]. The diffusivity K_y mainly depends on the barotropic instability of the mean zonal flow.

[21] For the simulations presented here, the model discretization is based on 48 latitude bands of equal width spread from pole to pole with 55 vertical layers of which the last three serve as a sponge layer to dump down the wind and prevent spurious reflection of waves. Level 52 is at approximately 480 km above the surface. The vertical resolution is about 3 km in the troposphere, 5 km at the tropopause and 10–15 km in the stratosphere, which corresponds to one half to one third of a scale height. The dynamical equations are integrated with a time step of 3 minutes. The radiative transfer is computed ten times per Titan day. Additional information is given by *Luz et al.* [2003b] and *Rannou et al.* [2004].

[22] All the simulations presented here were started from an initial state inherited from previous pluriannual simulations. The model was integrated for several Titan years and it was checked at the end, by comparing two successive years, that the results presented were identical. It appears in fact that the time constants involved when studying the stratospheric dynamics and composition are relatively short. In particular, the time constants for composition are not determined by the reaction rates themselves, which can correspond to very long time constants, but rather by transport and condensation close to the tropopause as analyzed in detail below. Finally, the results presented below for sensitivity experiments correspond to year 6, which is more than enough to obtain stable results from one year to the other.

2.4. Impact of Coupling on the Dynamics

[23] The first important result of the coupled model was to explain the origin of the detached haze layer observed in Voyager images above the main haze layer and to predict a strong accumulation of haze in the polar night [*Rannou et al.*, 2002]. This accumulation in turn increases radiative cooling to space in high latitudes, enforcing the meridional forcing of the general circulation [*Rannou et al.*, 2004] and hence latitudinal temperature contrasts and the zonal circumpolar jet, in better agreement with observations. The coupling with chemistry has a similar effect but occurs higher in the atmosphere, and is less sensitive for comparison with available observations [*Lebonnois et al.*, 2003b].

[24] As an illustration, we show in Figure 2 the comparison between the simulated and observed zonal wind profiles (comparison with the occultation profiles close to northern summer solstice [*Hubbard*, 1993]) and latitudinal temperature profiles at 1 hPa (compared with Voyager retrieval close to northern spring equinox by *Flasar et al.* [1981], *Flasar and Conrath* [1990], and *Coustenis and Bézard* [1995]). The comparison is shown for two simulations, one without coupling and another with the dynamics

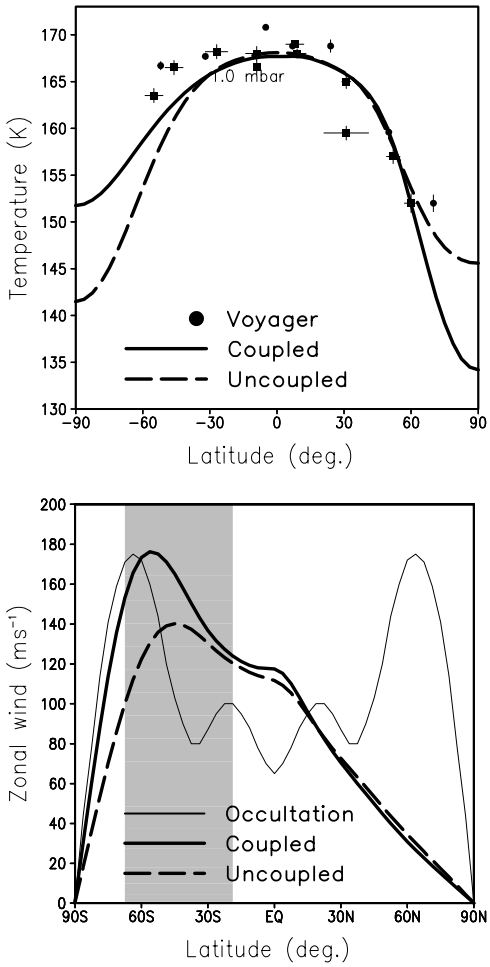

Figure 2. Stratospheric temperature (at 1 hPa, L_s = 9) and zonal winds (at 0.25 hPa, L_s = 128). Comparison between observations and simulations with and without coupling with the atmospheric chemistry and haze microphysics. Temperatures were retrieved from infrared remote sounding by Voyager shortly after northern spring equinox. The observed wind profile was deduced from the 1989 stellar occultation. The symmetric shape is imposed by the retrieval procedure, but observations are reliable only in the shaded area.

coupled with both haze and chemistry. The temperature contrasts in winter mid latitudes and the jet speed are in much better agreement for the coupled case.

2.5. North-South Temperature Asymmetry

[25] Note also that the coupled simulation tends to produce a north-south asymmetry of temperatures (top panel of Figure 2) consistent with Voyager observations. Voyager observed, shortly after northern spring equinox, a warmer southern hemisphere. This observation was a surprise since radiative time constants were estimated to be much shorter than a season at the pressure levels sounded by the methane bands. It was first suggested that this asymmetry could be due to a phase lag in the latitudinal redistribution of angular momentum by the mean meridional circulation [*Flasar and Conrath*, 1990]. Full simulations with a radiative convective model plus seasonal cycle showed in fact that the radiative time constants were long enough to explain the observed asymmetry. However, latitudinal redistribution of heat by dynamics would reduce instead of increase the asymmetry [*Hourdin et al.*, 1995]. On the basis of radiative computations, it was then suggested that the latitudinal variations in atmospheric composition and the north-south asymmetry in the haze distribution could cause the observed asymmetry [*Bézard et al.*, 1995]. The results obtained with the coupled and uncoupled models favor the second explanation. The coupling with dynamics, and the enrichment in haze and chemical compounds in the winter hemisphere, clearly contribute to the seasonal lag in atmospheric temperatures. However, the model still slightly underestimates the temperature at southern latitudes. So some additional dynamical or radiative effects, not well resolved by the model, can not be completely ruled out.

3. On Polar Enrichment

[26] The rationale behind enrichment in most chemical compounds in northern high latitudes at the time of the Voyager encounter (close to northern spring equinox) is as follows, and is illustrated in Figure 3. During almost half a year around solstice, the mean meridional circulation is dominated by a global pole-to-pole Hadley cell with the rising branch in the summer (southern) hemisphere and subsiding motions in the winter (northern) latitudes (arrows in Figure 3a). The downward advection of chemical compounds from the production zone in the upper stratosphere or mesosphere is responsible for the strong polar enrichment [*Lebonnois et al.*, 2001] as illustrated for HCN in Figure 3a (shaded). This Hadley circulation also creates an intense circumpolar jet in northern high latitudes (shaded in Figure 3b). This jet is unstable on its equatorward flank leading the development of planetary waves. Those waves, parameterized in the model [*Luz et al.*, 2003b], are responsible for the erosion of the polar bulge. Values of the parameterized eddy diffusivity K_y averaged for northern winter are shown in Figure 3b (contours). Figure 4 summarizes these mechanisms.

3.1. Composition of the Polar Vortex

[27] For the simulations with linearized chemistry, the time evolution of the mass concentration c of a given chemical compound is simply given by

$$\frac{\partial c}{\partial t} + v\frac{\partial c}{a\partial \phi} + w\frac{\partial c}{\partial z} = \frac{c_0 - c}{\tau_{\text{chem.}}} + \frac{1}{a^2 \rho \cos\phi}\frac{\partial}{\partial \phi}\left(\cos\phi \rho K_y \frac{\partial c}{\partial \phi}\right), \quad (1)$$

where ϕ is the latitude, z is the altitude, ρ is the air density, a is the radius of Titan, v and w are the meridional and vertical wind components, K_y is the lateral eddy diffusivity defined above, c_0 is a one-dimensional vertical profile determined from a one-dimensional simulation of Titan's photochemistry and $\tau_{\text{chem.}}$ is a time constant from the same simulation which also depends on altitude only [*Lebonnois et al.*, 2001].

[28] For chemical species subsiding in the polar vortex down from the production zone, the concentration decreases under the combined effects of meridional advection of clear air from low latitudes and latitudinal mixing by waves. By

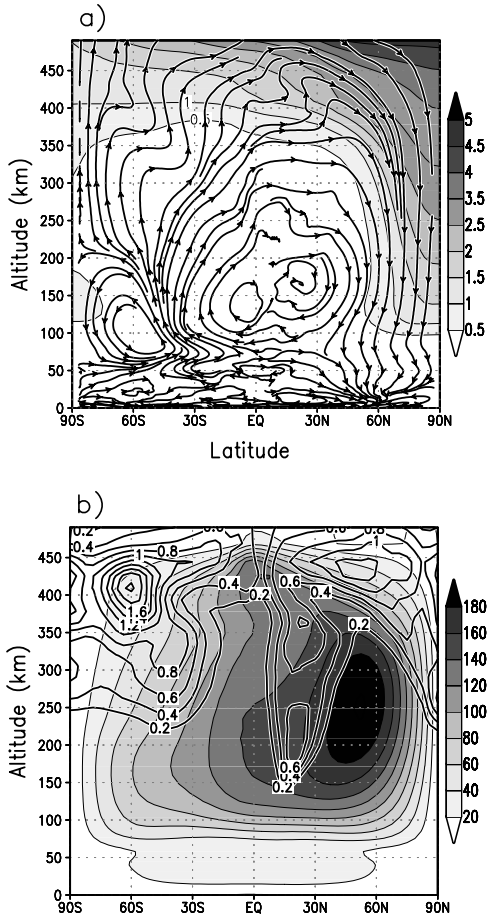

Figure 3. Meridional transport of HCN during northern winter. (a) Meridional cross section of HCN concentration (in ppmv) (shaded) with stream lines of the mean meridional circulation (black arrows). (b) Zonal wind (shaded) and latitudinal eddy diffusivity K_y (contour, 10^{-6} m^2 s^{-1}). With these particular units, the same contours can be interpreted as well as iso-values of a meridional eddy velocity in m s^{-1} for a mixing length of 1000 km. All the quantities are averaged from northern winter solstice to northern spring equinox.

denoting by c_{eq} the typical concentration at low latitudes, the erosion of the polar vortex concentration c by latitudinal eddy diffusion (last term in equation (1)) can be roughly estimated as

$$\frac{K_y}{l^2}\left(c_{eq}-c\right), \tag{2}$$

where $l \simeq 1000$ km is the typical length scale associated with latitudinal contrasts in atmospheric composition. Similarly, the effect on the polar vortex concentration c of advection of clear air from low latitudes by a meridional wind v (assumed positive in the northern hemisphere), $(-v/a)\partial c/\partial\phi$, can be approximated as

$$\frac{v}{l}\left(c_{eq}-c\right). \tag{3}$$

Assuming a steady state regime, the transport equation can be approximated as

$$w\frac{\partial c}{\partial z} \simeq \frac{c_0-c}{\tau_{chem.}} + \left(c_{eq}-c\right)\left(\frac{K_y}{l^2}+\frac{v}{l}\right). \tag{4}$$

For a large number of species, the polar enrichment is such that the hypothesis that $c_0 \ll c$ and $c_{eq} \ll c$ can be made. In such conditions, and for a positive meridional wind $v > 0$, the vertical gradient of c in the polar vortex is given by

$$w\frac{\partial c}{\partial z} \simeq -c\left(\frac{1}{\tau_{chem.}}+\frac{K_y}{l^2}+\frac{v}{l}\right), \tag{5}$$

corresponding to a total atmospheric scale height for the mass concentration of

$$H = \left(\frac{d\ln c}{dz}\right)^{-1} \simeq -w\left(\frac{1}{\tau_{chem.}}+\frac{K_y}{l^2}+\frac{v}{l}\right)^{-1}. \tag{6}$$

For species with large chemical time constants (compared to dynamical time constants), the shape of the vertical concentration profile is controlled by a competition between vertical advection (with faster advection from the upper stratosphere reducing vertical contrasts) and relaxation toward the weak concentrations found in low latitudes in the mid stratosphere by either mean meridional transport or latitudinal mixing by waves (which accentuates the vertical contrasts). The relative importance of meridional advection and latitudinal mixing can be quantified either in terms of time constants, $\tau_{mmc} = l/v$ and $\tau_{mix} = l^2/K_y$ or in terms of the associated scale height $-w\tau_{mmc}$ and $-w\tau_{mix}$.

[29] In Figure 5a, we show for northern winter (quantities averaged between northern winter solstice and northern spring equinox) the time constants for the vertical and meridional advection as well as for latitudinal mixing by

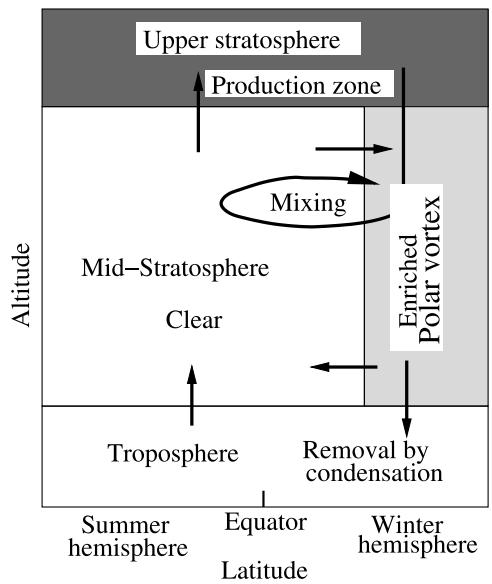

Figure 4. A sketch of the essential mechanisms responsible for the observed contrasts in Titan's stratospheric composition.

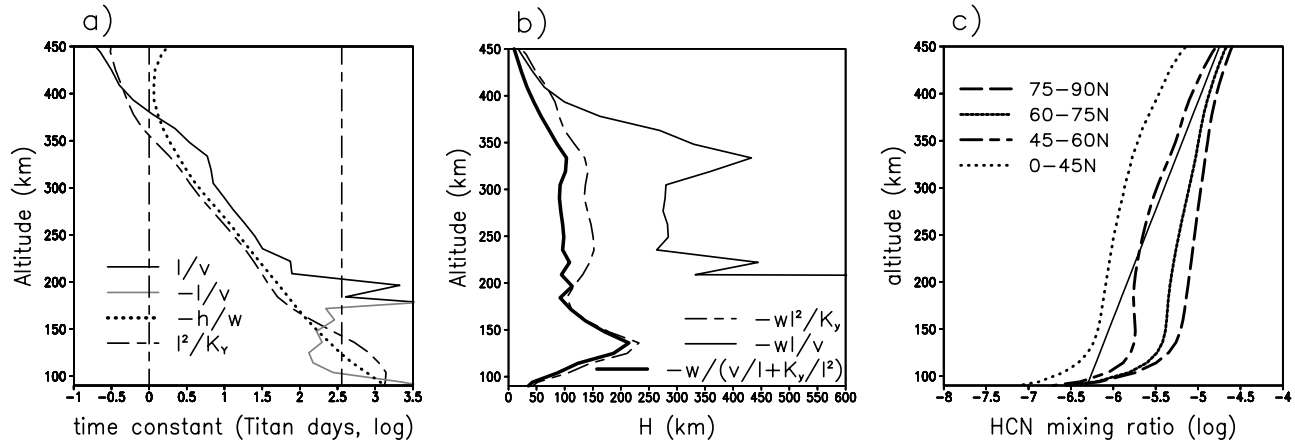

Figure 5. Time constants and vertical profiles in the winter polar vortex. (a) Time constants (in Titan days) for vertical advection in the core of the vortex ($-h/w$, with h = 150 km, averaged between 70 and 90N), and meridional circulation (l/v, with l = 1000 km, averaged between 50 and 80N) and latitudinal mixing by waves (l^2/K_y, averaged between 50 and 80N) at the edge of the vortex. The gray curve corresponds to meridional advection toward the equator ($-v$ instead of v). The vertical lines correspond to 1 day and 1 year. (b) Associated scale height (km) for meridional advection, $-wl/v$, latitudinal mixing $-wl^2/K_y$, and the total scale height $H = -w/(v/l + K_y/l^2)$. (c) Vertical profiles of the mole fraction of HCN (in log scale) at different latitudes (linearized chemistry). The thin oblique line corresponds to a constant scale height of 100 km.

waves. The meridional advection dominates latitudinal transport only in the upper branch of the Hadley cell (above 400 km) as well as in the lower stratosphere, between 100 and 150 km were the meridional wind is negative. This region corresponds to the lower branch of the stratospheric Hadley cell. Typical values for dynamical time constants vary from about one Titan year at 120 km to less than one Titan day above 350 km. As discussed below, those time constants are shorter or much shorter than chemical time constants for most species. The associated dynamical scale height (Figure 5b) is of the order of 100 km in the mid-stratosphere, where it is essentially determined by the balance between downward advection and latitudinal mixing by waves.

[30] Figure 5c shows, at the same season, simulated vertical profiles of HCN (obtained with the linearized chemistry) for different latitude ranges in the northern hemisphere. The straight line in the same panel corresponds to a scale height of 100 km. This is very close to the scale height for HCN profiles above 250 km at 45–60N, at the edge of the polar vortex, in the region of mixing. Between 100 and 150 km, the scale height is much larger due to the weaker mixing there. For the 45–60N profile, a local maximum is even obtained in this altitude range, due to meridional advection of rich air from the polar vortex.

[31] The shape of the vertical profiles, with three distinct slopes and a very well mixed region in the mid-stratosphere, between 150 and 400 km, is consistent with recent observations by *Marten et al.* [2002]. Numerical simulations with one-dimensional chemical models show much larger vertical variations in this region due to a much weaker vertical transport [see, e.g., *Hidayat et al.*, 2002, Figure 1]. The vertical advection by the stratospheric Hadley cell is in fact much more efficient in transporting chemical species over long distances than turbulent mixing by small scale eddies. For a vertical eddy diffusivity K_z and a vertical scale h, the time scale for diffusive mixing is h^2/K_z instead of h/w for advection. Between 250 and 150 km, the time constant associated with vertical advection varies from about 10 to 100 Titan days. Very large values of K_z of typically 100–5000 m^2 s^{-1} would be required (assuming $h \simeq 200$ km) to obtain similar time constants. This is consistent with the study by *Lebonnois et al.* [2003a] in which an eddy diffusion coefficient of 100 m^2 s^{-1} was adopted in this region to emulate mixing by the general circulation.

3.2. Magnitude of Latitudinal Contrasts

[32] The enriched subsiding air generally reaches saturation when approaching the tropopause level, explaining the sharp decrease observed in Figure 5c for HCN at all latitudes. For most species, the concentration at saturation at the very cold tropopause of Titan ($T \simeq 70$ K) is orders of magnitude smaller than the concentrations observed in the polar vortex. So the air which is recycled in low latitudes rises from the troposphere with a very low concentration. It is then replenished either by latitudinal advection from the polar vortex or by latitudinal mixing by waves. The latitudinal contrast observed for altitudes ranging from 80 to 200 km thus essentially represents the efficiency of mixing and latitudinal transport to carry chemical species into the clear air rising from the troposphere. As is visible in Figure 5, meridional advection dominates this latitudinal transport below 150 km (gray curve in Figure 5a).

[33] This simple idea of the buildup of latitudinal contrasts was checked by simulating chemical compounds as very simple atmospheric tracers (thereafter named idealized tracers). In the three upper layers, those tracers are relaxed (with the same time constants as for the linearized chemistry) toward a concentration of unity. The tracers undergo both the mean meridional circulation and latitudinal mixing, but not chemistry. The tracers are completely removed below a given level, close to the tropopause. The various

Table 1. Condensation Level, Polar Enrichment, and Chemical Time Constants for Various Chemical Compounds[a]

	C_2H_2	C_2H_4	C_2H_6	CH_3CCH	C_3H_8	C_4H_2	HCN	HC_3N
Condensation Level								
Winter polar vortex, km	64	-	57	64	54	77	86	63
Winter polar vortex, hPa	35	-	50	35	60	20	15	36
Retained for idealized tracers, hPa	40	-	80	40	100	20	20	40
Level of Maximum of the Weighting Function for Voyager IRIS Observations								
km	152	190	160	85	125	100	107	103
hPa	2.5	1	2	13	5	10	8	9
Polar Enrichment								
Observations	2.1	8.3	1.4	6.4	1.9	16.8	7.6	19.6
Full chemistry	2.7	3	1.9	9.9	1.6	5.9	7.8	6.2
Linearized chemistry	2.3	-	1.3	-	-	-	7.5	-
Null chemistry	2.6	2.6	1.9	9.6	1	10.1	9.2	5.2
Idealized tracers	2.4	-	2	5.6	2.6	9.3	9.3	4.2
Chemical Time Constant (Titan Year)								
0.5–1 hPa (190–200 km)	0.5–100	0.03–4	>40	2–100	>10	0.001–1	2–200	0.05–10
2–5 hPa (125–160 km)	>2.5	0.2–5	>200	2–200	>80	0.01–3	2–300	0.2–50

[a]Polar enrichment is the ratio of the averaged concentrations at 50–70N and 0–30N.

tracers only differ by the pressure level at which they are removed. We consider 8 idealized tracers corresponding to condensation levels of: 100., 80., 60., 40., 30., 20., 15. and 10. hPa. The idealized tracers can only be compared to real chemical compounds in terms of relative latitudinal or vertical variations. Also, because the idealized tracers disappear suddenly at the condensation level whereas the actual concentration is decreasing gradually in the condensation region, the level retained for the condensation of the idealized tracer must be somewhat lower than the real condensation level of the chemical compound to which it is compared (typically at the level where the concentration has decreased by one order of magnitude, which generally occurs at a little bit less than twice the pressure of the actual condensation level). The actual level of condensation in the winter polar vortex was computed from the simulation with full chemistry, as the upper layer where the given species condenses (note that this level depends on the concentration simulated for that species in the polar vortex). This level as well as the level retained for the idealized tracer is given for a certain number of species in Table 1.

[34] Table 1 also shows the polar enrichment, defined as the ratio of the averaged concentrations at 50–70N and 0–30N. First, the comparison of the observed polar enrichment with the results of the model with full chemistry shows an agreement for most species, except C_2H_4 – the enrichment appears closer to the pole than observed – C_4H_2 and HC_3N – which may be affected by chemical processes not included in the model (e.g., pathways producing haze precursors). For most species (C_2H_2, C_2H_6, C_3H_8, HCN, HC_3N), the polar enrichment obtained for the full chemistry and idealized tracers differ by less than 50%. This general agreement clearly shows that the level at which species are removed by condensation is controlling for a large part the magnitude of polar enrichment. The secondary role played by either chemistry or specifications of the model upper boundary conditions is detailed below.

[35] In order to estimate the relative importance of chemistry for the various species, we computed a chemical time constant $(d\ln c/dt)^{-1}$, where the tendency is computed for all the chemical reactions acting as a sink for the given species. Values are given for two pressure ranges in Table 1. We also ran the full chemical model but replacing all chemical rate constants by zero (thereafter named null chemistry; see Table 2). Values of the polar enrichment obtained by the full and null chemistry depart by less than 20% except for C_4H_2 and C_3H_8. The disagreement between null and full chemistry for C_4H_2 is consistent with the relatively short chemical time constants obtained for this species. In the case of C_3H_8, the discrepancy between full and null chemistry, despite very long chemical time constants, is probably due to the fact that the flux at the upper boundary is very close to zero. This flux is probably underestimated by the one-dimensional photochemical model, leading to an underestimated equatorial value in the GCM. The photochemical reactions, though occurring on long timescales, may then explain the difference between both simulations (Table 1). As a consequence also, the simulation of C_3H_8 as an idealized tracer, with an upper condition prescribed as a relaxation toward a fixed value, also departs from the null chemistry.

[36] For the other species, the agreement between the null chemistry and idealized tracer is very good, in spite of the different treatment of the upper boundary condition and of the condensation (see summary of the different simulations in Table 2). This good agreement reinforces the confidence in the results presented above. In particular, the upper boundary condition which, for a given species, controls its mean level in the lower stratosphere, does not affect its latitudinal variations.

[37] Finally, it clearly appears that the level of condensation is the main determinant of the magnitude of polar enrichment for most species. The higher the condensation occurs the stronger the polar enrichment. If the observa-

Table 2. Characteristics of the Various Chemical Schemes

Simulation Name	Chemistry	Condensation	Upper Boundary Condition
Full chemistry	realistic	realistic	prescribed flux
Null chemistry	no	realistic	prescribed flux
Linearized chemistry	relaxation	realistic	relaxation
Idealized tracers	no	removal below a given pressure level	relaxation

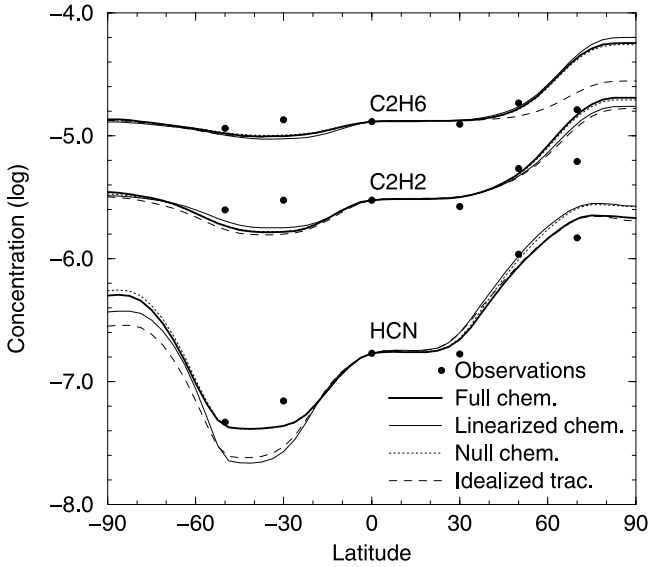

Figure 6. Latitudinal profiles of chemical species as computed with the 4 options (full, linearized, or null chemistry as well as idealized tracers) compared to Voyager observations. Curves are normalized to the observed equatorial value to focus on latitudinal variations.

tional contribution function peaks just above the condensation level, the observed polar enrichment will also be larger than if the contribution function peaks much higher in the atmosphere. This for instance explains the small polar enrichment of C_2H_2 when compared to CH_3CCH, while both condensate at the same levels.

[38] The same processes explain not only the magnitude of the polar enrichment but also the shape of the latitudinal profiles. To illustrate this point, we show in Figure 6, for the three radiatively active species, the latitudinal profiles normalized to the observed equatorial value for the various simulations. We compare normalized rather than absolute profiles to focus on latitudinal variations and also because comparison of absolute values does not make sense for the idealized tracers which are arbitrarily relaxed toward a concentration of unity at the model top (comparisons of absolute profiles are shown in Figure 1 for the full and linearized chemistry). The agreement between all those profiles, from the most complex with full chemistry to the simple idealized tracer, clearly confirms the very weak control by chemistry of those latitudinal variations.

4. Constraints on Winds

[39] If the latitudinal contrasts depend primarily on dynamics as well as on the level of removal by condensation for each species, what does observation of the composition tells us about winds? Or, to which degree is the agreement with observations sensitive to the simulated circulation?

[40] To answer that question, we made a series of sensitivity experiments by varying the intensity of either the meridional advection or latitudinal mixing. A factor was applied either on both v and w or on the eddy diffusivity K_y, with two values: 0.3 and 3. The factor was applied for the transport of the three linear chemical species only.

[41] We also performed simulations with and without coupling with chemistry or haze microphysics. The coupling with haze is turned off by applying a strong latitudinal mixing on haze particles to obtain almost no latitudinal contrasts. In those simulations, the production rate of haze must be strongly reduced to obtain the same geometric albedo of Titan (see *Rannou et al.* [2004] for additional details). In the radiative computation, coupling with chemistry is turned off by using the *Lellouch et al.* [1989] vertical profile of the methane abundance, and values taken from *Coustenis et al.* [1989] for ethane and acetylene above their condensation level. In this simulation however, the chemical compounds are transported as in the coupled version. Note that, to avoid complex feedbacks which would complicate the analysis, the simulations with modified meridional circulation or latitudinal mixing are performed without coupling with chemistry.

[42] In Figure 7, we compare the polar enrichment for C_2H_2 and HCN obtained in the various sensitivity experiments and in Voyager observations (with associated error bars). For the nominal version, the latitudinal contrast is very well reproduced for both species. The ratio is much larger (respectively weaker) if the meridional advection (v and w components) is increased (respectively decreased) or if the latitudinal mixing is weakened (respectively strengthened). So observations of the composition actually contain strong constraints on the combined intensity of advection and mixing. The results suggest that those components are predicted at a factor of typically less than two with the nominal version of our coupled Titan GCM.

[43] Coupling with chemistry tends to degrade a little bit the agreement but keeps the results in the error bars.

[44] Without haze coupling, the agreement is significantly reduced, the contrast for HCN being much too low and that of C_2H_2 too high. The difference in sensitivity of these two species is due to the level at which they are observed. In Figure 8, we show a latitude-altitude cross section of the

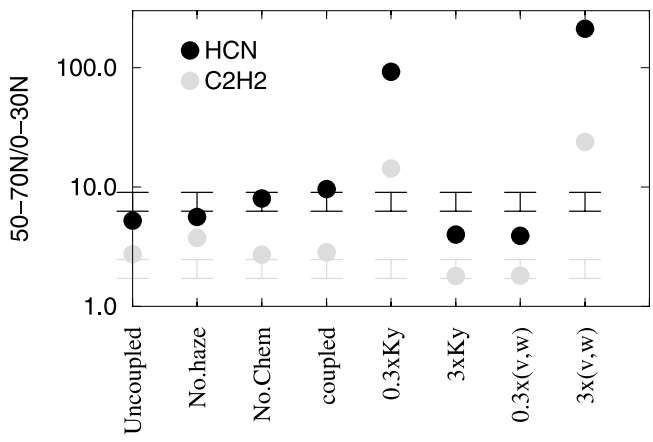

Figure 7. Sensitivity experiments. Polar enrichment in C_2H_2 and HCN obtained with the full coupled model, or with uncoupled chemistry (No chem) or uncoupled haze (No haze) or both (uncoupled) or with weakened (0.3xKy) or enhanced (3xKy) dissipation by waves or modified advection field for chemical compounds (mean meridional circulation multiplied by 0.3 or 3). The error bars correspond to the Voyager data.

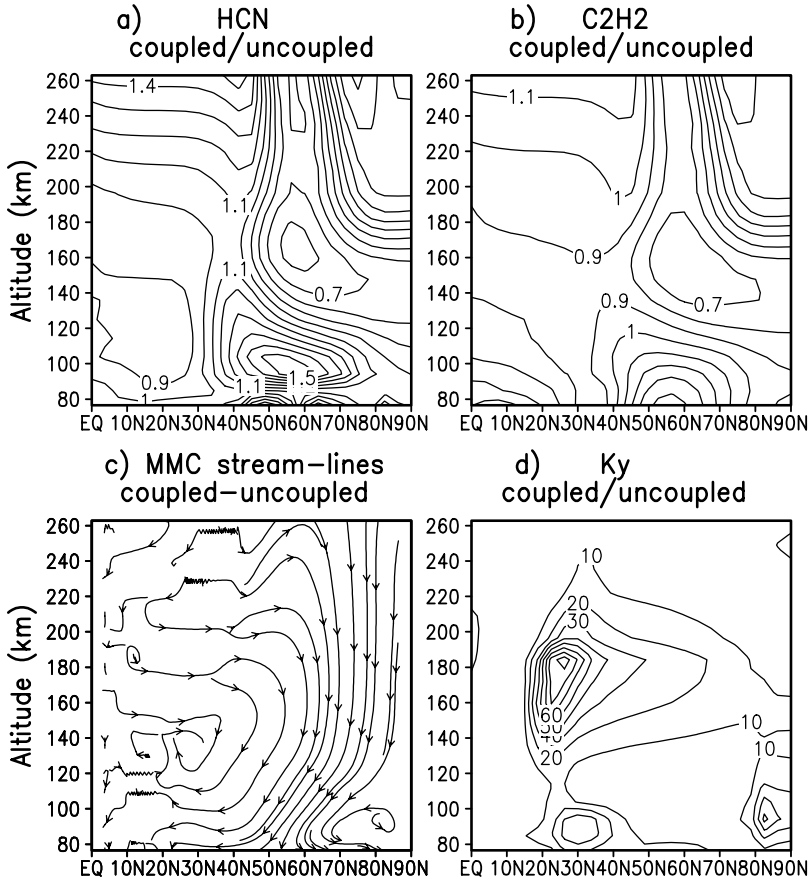

Figure 8. Effect of the coupling with the haze on the latitude-altitude distribution of (a) HCN and (b) C_2H_2 and associated impact on the (c) mean meridional circulation (MMC) and (d) latitudinal eddy diffusivity K_y (10^{-6} m^2 s^{-1}) at the time of the Voyager encounter.

ratio of the concentrations of HCN (Figure 8a) and C_2H_2 (Figure 8b) in the coupled and uncoupled simulations at the time of the Voyager encounter. The sensitivity is in fact very similar for the two species, with a decrease by about 30% in the polar vortex near 160 km and an increase by about 50% near 100 km, and can be interpreted as follows.

[45] The main effect of coupling with haze is a reinforcement of the subsidence in the winter polar region, due to a larger infrared cooling to space due to the accumulation of haze in the polar night [*Rannou et al.*, 2004]. This reinforcement of the meridional circulation is illustrated by the stream-lines in Figure 8c. It is responsible for the increase in concentration in the low stratosphere, near 100 km. At the same time, the stronger jet in the coupled version leads to stronger wave activity (Figure 8d). The latitudinal eddy diffusivity is much larger in the coupled version. This reinforcement is particularly strong near 150 km and explains the weaker polar enrichment in this altitude range in the coupled model.

[46] C_2H_2 which is observed at 2.5 hPa, close to 160 km, has a smaller polar enrichment in the coupled version while it is the opposite for HCN which is observed close to 100 km.

5. Seasonal Variations

[47] We have focused up to now on the mean winter conditions for interpreting the physics of the transport of chemical compounds and on northern spring equinox for the comparison with Voyager observations.

[48] In Figure 9 we present how the northern polar enrichment in HCN, as well as the associated components of atmospheric transport, evolve with seasons in the mid stratosphere (80–240 km).

[49] Soon after fall equinox in this altitude range, the high-latitude concentration grows very fast under the effect of downward advection (Figure 9a). At the same time, the jet is not yet established so that the latitudinal contrasts with low latitudes grow very fast, reaching a first maximum (Figure 9c). The polar enrichment then decreases under the combined effect of mixing by waves and latitudinal advection from the vortex toward low latitudes. Close to northern spring equinox, the meridional advection reverses above 150 km. The chemically rich air of the polar vortex is then rapidly advected toward the other hemisphere, explaining both the rapid decrease of concentrations at 50–70N above 180 km (Figure 9a) and the local maximum observed at 0–30N, in the upper part of the domain of Figure 9b. In the lower part, the polar high concentrations persist much longer, both because the time constants are longer there, and because the vertical and meridional advection do not change their signs in high latitudes.

[50] Around equinox on the other hand, the ascending branch of the stratospheric Hadley cell migrates from the hemisphere coming out of summer to the other hemisphere,

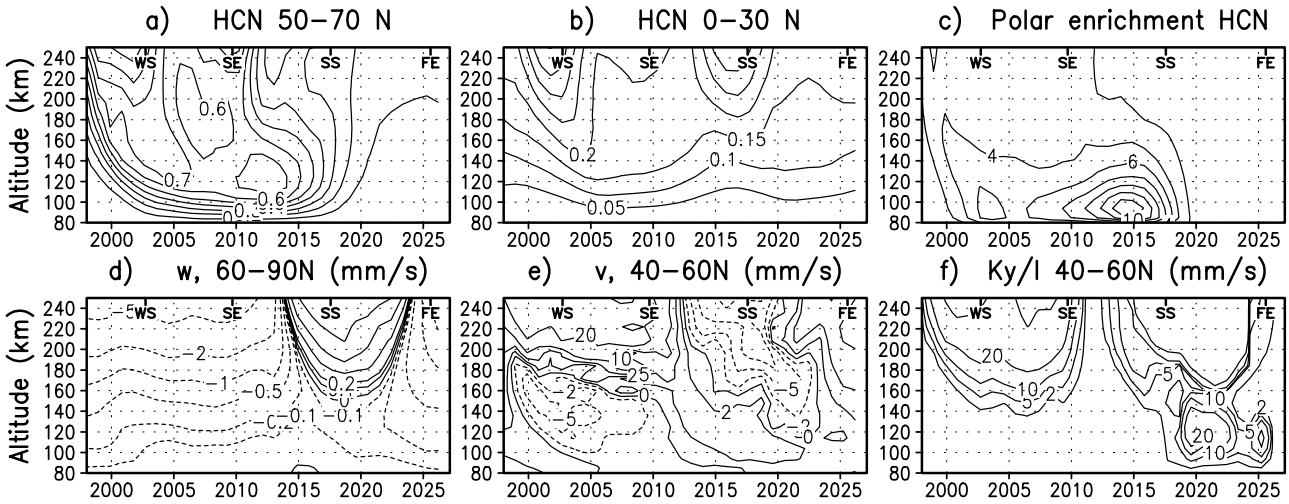

Figure 9. The seasonal evolution of the concentration of HCN (ppmv) at (a) 50−70N and (b) 0−30N as well as (c) the corresponding polar enrichment are shown, together with the various components of atmospheric transport: (d) vertical wind in the polar vortex as well as (e) meridional wind and (f) latitudinal mixing at the edge of the polar vortex. The lower time axis is in terrestrial years. Titan seasons are also indicated: WS is for winter solstice, SE is for spring equinox, SS is for summer solstice, and FE is for fall equinox.

bringing clear tropospheric air to the lower stratosphere at low latitudes. This upward advection of clear air explains the decrease observed below 150 km at 0−30N (Figure 9b) and the associated maximum in polar enrichment (Figure 9c). At this season also, the intensity of latitudinal mixing reaches a minimum in the lower stratosphere. But, as already stated, it is essentially the mean meridional advection which controls the polar enrichment below 150 km (compare Figures 9e and 9f). The time constant of about 5 terrestrial years which can be deduced from the decrease of the first maximum of polar enrichment (Figure 9c) is also the time it takes to travel 1000 km at a speed of 5 mm s^{-1}, which is the typical meridional velocity encountered in the lower branch of the stratospheric Hadley cell, near 120 km (Figure 9e).

[51] This seasonal evolution is illustrated in a series of 6 snapshots running from northern fall to northern spring equinox (Figure 10). At both equinoxes (first and last panels) the upward advection of clear air by the low-latitude branch of the two equator-to-pole Hadley cells is clearly visible. At fall equinox (Figure 10a), the southern polar vortex is still strongly enriched while the rich air from the upper stratosphere starts to sink in the northern high latitudes. Then the global pole-to-pole Hadley cell sets in (Figures 10b−10d), with an ascending branch in the south and subsidence in the north. Between 80 and 200 km, a secondary Hadley cell appears in the summer hemisphere which persists until the next equinox. This secondary cell clearly contributes to maintain a strong enrichment in the summer hemisphere, in the lower stratosphere.

[52] Note that this secondary cell is much more intense when the circulation is coupled to the haze.

[53] Because of this secondary cell also, the air keeps on sinking into the troposphere during summer, producing condensation at high latitudes (condensation is shown as shaded squares close to 80 km altitude in Figure 10), even close to summer solstice when insolation is maximum at the pole. Exactly the same picture is obtained with C_2H_6 and C_2H_2 (not shown). Condensation in the polar branch of this secondary cell is in fact the sink of polar enrichment in the lower stratosphere during summer. This may also explain the cloudy features observed around the pole during summer from ground-based observations [*Griffith et al.*, 1998, 2000; *Brown et al.*, 2002; *Roe et al.*, 2002b] and more recently from the T0 Cassini flyby of Titan. Our results clearly show that there is no contradiction between the season (summer) and a stratospheric origin of the observed clouds, so that a convective origin from the troposphere is not required. From our computation, it appears that clouds are as likely in the summer as in the winter hemisphere.

6. What Should Cassini Observe?

[54] Most that is known about the composition and dynamical state of Titan's mid stratosphere (pressure range 10−0.1 hPa) comes from the Voyager observations, at northern spring equinox. The vertical temperature profile, from the surface up to 200 km was reconstructed from radio occultation measurements [*Lindal et al.*, 1983]. From there upward it is mainly constrained by the model by *Yelle et al.* [1991]. For stratospheric dynamics, an estimate of the zonal flow was inferred through geostrophic balance [*Flasar et al.*, 1981] from the temperatures retrieved for two pressure levels (0.4 and 1 hPa) from observations of the Q and P branches of the ν_4 band of methane by the Voyager Infrared Spectrometer (IRIS). Since then, ground-based observers have tried to measure zonal winds with two main techniques: stellar occultations [*Hubbard*, 1993; *Bouchez et al.*, 2003a], which provide the speed but leave the wind direction undetermined, and from the Doppler shifts of either ethane and nitrile emission lines [*Kostiuk et al.*, 2001; *Moreno and Marten*, 2003] or of the backscattered solar spectrum [*Luz et al.*, 2003a].

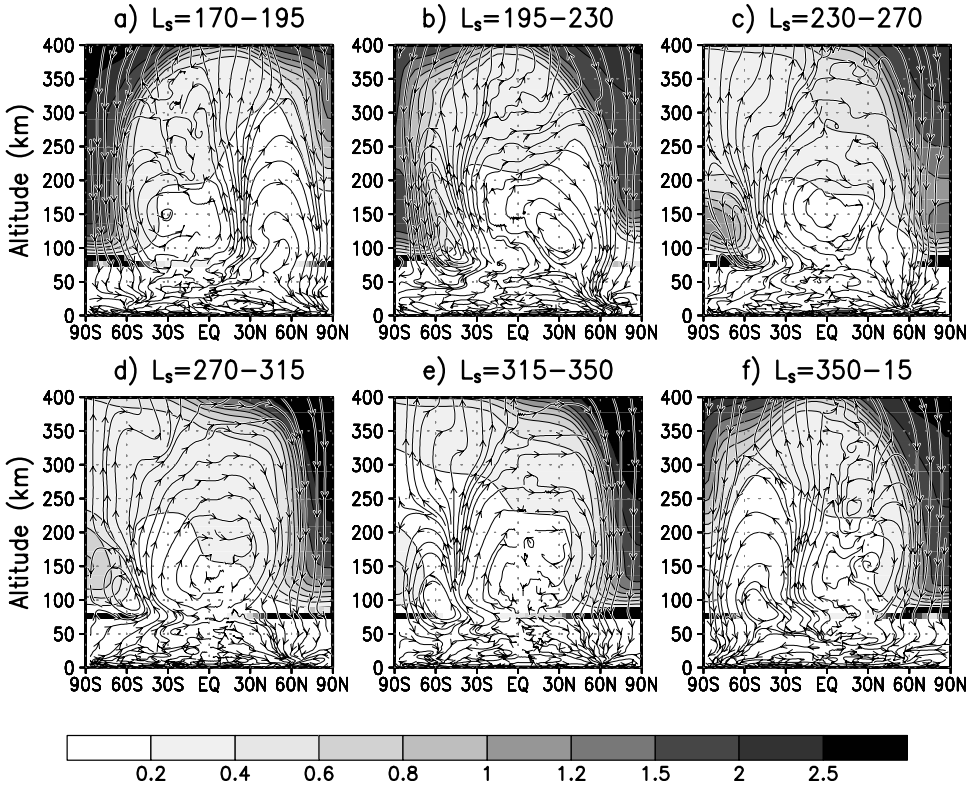

Figure 10. Six snapshots of the meridional structure for HCN and associated mean meridional circulation for seasons going from northern fall to northern spring equinox. Seasons are labeled according to the solar longitude L_s with $L_s = 180$ for northern fall equinox, $L_s = 270$ for northern winter solstice, and $L_s = 0$ for northern spring equinox. Concentration of HCN (gray scales) is in ppmv. The condensation rate of HCN is shown as shaded squares with the same bar chart but for 10^9 molecules m^{-3} s^{-1}.

[55] The stratospheric composition is also constrained from Voyager IRIS observations. The equatorial composition has been obtained in the region 80–200 km for several hydrocarbons and nitriles (C_2H_2, C_2H_4, C_2H_6, CH_3C_2H, C_3H_8, C_4H_2, HCN), and latitudinal variations of their abundances could be retrieved thanks to the latitudinal resolution of IRIS [*Coustenis et al.*, 1989; *Coustenis and Bézard*, 1995]. Ground-based observations made since only give access to a mean stratospheric value (C_2H_6 [*Livengood et al.*, 2002]; C_3H_8 [*Roe et al.*, 2003]) or to a mean stratospheric vertical profile (HCN, CH_3CN, HC_3N [*Marten et al.*, 2002]), which as mentioned above also contains information on atmospheric dynamics.

[56] Latitudinal contrasts in haze also contain information on dynamics. They have been monitored by Voyager [*Sromovsky et al.*, 1981] and, since then, by the Hubble Space Telescope [*Lorenz et al.*, 1999, 2001; *Young et al.*, 2002] and ground-based observatories with adaptive optics and speckle imaging [*Roe et al.*, 2002a; *Gendron et al.*, 2004; *Gibbard et al.*, 2004]. Transient cloud features have been detected from disk-integrated infrared spectra [*Griffith et al.*, 2000], and from resolved adaptive optics [*Brown et al.*, 2002; *Roe et al.*, 2002b] and speckle imaging [*Gibbard et al.*, 2004]. Haze aspects of our simulations are already published [*Rannou et al.*, 2002, 2004]. Although strongly coupled to dynamics, the distribution of haze and clouds are much more sensitive to the way the microphysics is handled than chemical composition. Thus constraints on the dynamics are less direct than for chemical compounds.

[57] The Cassini orbiter has been placed in Saturn's orbit on the 1st of July 2004. During four years it will make several Titan flybys, which will be used to modify the orbits around Saturn. It will monitor at least a part of the seasonal cycle. Information on the dynamics of the mid-stratosphere will be provided essentially by observations of thermal contrasts by the composite infrared spectrometer (CIRS), but recent observations by the Imaging Science Subsystem (ISS) indicate that cloud tracking may become a possibility. The Doppler Wind Experiment (DWE) on board the Huygens probe will measure the speed and direction of the winds to better than 1 ms^{-1} accuracy during the descent [*Bird et al.*, 2002], but only below 160 km and in a very limited time span. Both the Descent Imager/Spectral Radiometer (DISR) and the Huygens Atmospheric Structure Instrument (HASI) data sets will also allow to corroborate DWE measurements [*Allison et al.*, 2004; *Fulchignoni et al.*, 2002].

[58] Here we propose some predictions of what we expect Cassini-Huygens to observe in Titan's mid stratosphere. Of course the model could predict a number of things. In Figure 11, we show predictions concerning quantities which were observed by Voyager but at a different season. We first show the seasonal evolution of polar enrichment for HCN and C_2H_2, for altitudes corresponding to the maximum of the weighting function of Voyager infrared retrievals

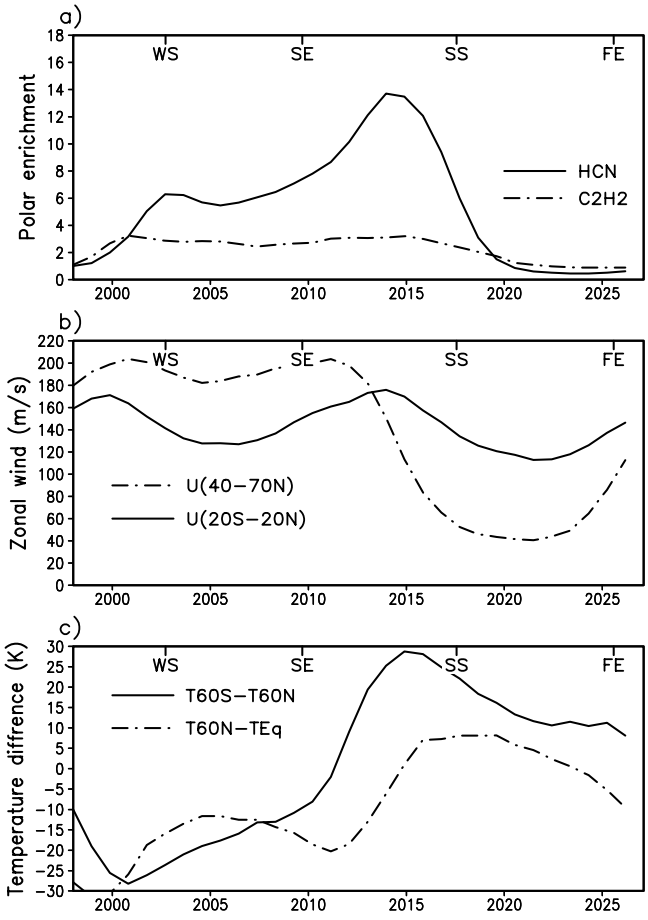

Figure 11. Time evolution of some observable quantities. (a) Polar enrichment for HCN (at an altitude of 107 km) and C_2H_2 (at 152 km). (b) Zonal wind at the equator (20S–20N) and in the northern high-latitude jet (40–70N) at an altitude of 250 km. (c) Equator to high-latitude (60N) temperature contrast and north-south asymmetry (temperature difference between 60N and 60S) at 190 km.

(107 and 152 km respectively). The two-peak maximum described above is clearly visible for the polar enrichment of HCN (Figure 11a). For C_2H_2, the second maximum is not visible not because of a different condensation height, but rather because of the higher altitude probed. Note also that the enrichment for HCN increases with a phase lag of 1–3 terrestrial years with respect to C_2H_2, at the beginning of fall. This phase lag is directly related to the difference in altitude of the two weighting functions (50 km lower for HCN). The corresponding downward velocity in the polar vortex is of the order of 0.5–1.5 mm s^{-1}, which is consistent with the values given in Figure 9. Here, the vertical wind can be deduced almost directly from the observation of the atmospheric composition.

[59] In the second panel, we show the time evolution of the stratospheric jet speed (40–70N) and equatorial zonal wind velocity at 250 km. It is not clear whether Cassini will succeed in measuring directly the winds by tracking clouds or other structures, since, except for recent ground-based detections of clouds at the south pole, Titan's disk seems featureless. However, the 250 km-altitude range is interesting because it can be probed by stellar occultations (including the 2003 occultation, B. Sicardy, private communication) and by heterodyne infrared spectroscopy [*Kostiuk et al.*, 2001]. The time evolution of the stratospheric jet presents similarities with that of HCN, with a two-maxima structure and a long winter season with an intense circumpolar jet, contrasting with a shorter season where the wind speed is less than the equatorial velocity.

[60] The time evolution of the latitudinal temperature contrast at 1 hPa or 190 km, which will be easily monitored by Cassini, is still more complex. The polar latitudes are generally colder than the equator except during a short season around the summer solstice.

[61] The curves shown in Figure 11 are relative to the northern hemisphere but the situation is, to first order, symmetric for the southern hemisphere (not exactly because of the eccentricity of Titan's orbit around the Sun) so that the situation at the time of arrival is given by year 2005 for the northern hemisphere and 2020 for the southern hemisphere. According to those figures, Cassini should arrive at the time at which the zonal winds are weakest in the southern hemisphere, with southern high latitudes warmer than the equator.

[62] As shown in Figure 9f, it should be a period of intense wave activity. From Figure 5, it is seen that the time constants of latitudinal mixing and vertical advection are of the order of tens of Titan days in the mid stratosphere. According to the simulations of latitudinal mixing by planetary waves presented by [*Luz and Hourdin*, 2003], longitudinal contrasts less than 10% of the latitudinal contrasts are expected, which could be monitored as well by Cassini's CIRS.

[63] Many other quantities will be observed by remote sounding by Cassini and in situ measurements by the Huygens descent module. A database based on a reference simulation performed with the coupled model is now distributed to the scientific community (http://www.lmd.jussieu.fr/titanDbase), so that it will be possible to check a posteriori if the observations confirm or not other components of the simulations.

7. Concluding Remarks

[64] The results presented above have been obtained with a state-of-the-art comprehensive climate model of Titan, including coupling with both chemistry and haze microphysics. This model, however, presents a number of approximations and limitations which must be kept in mind when discussing the results. First, the model is reduced to an axisymmetric version. Latitudinal mixing by waves is handled through a parameterization which obviously only partially and imperfectly reproduces the physics of these waves. In particular, there was no attempt to predict mixing by baroclinic waves which may become significant at high latitudes. Also, because of the two-dimensional nature of the model as well as of the lack of information on surface conditions, longitudinal forcing, as could occur from the presence of mountains, is not included. Subgrid scale gravity waves, which could be parameterized as in many terrestrial or Martian GCMs, are not accounted for either, once again essentially because of the lack of information on the possible sources. The dynamical core of the model is

based on the primitive equations of meteorology, which assume the thin layer approximation, whose validity becomes doubtful at altitudes as high as 400 km on Titan. The thin layer approximation could in particular affect the magnitude of superrotation since the altitude with respect to the surface is not taken into account when computing the distance to the polar axis which enters in the definition of angular momentum. Because of this approximation, an overestimation by 10% of the zonal wind can be expected at the peak altitude for superrotation, near 300 km. At the model upper boundary also, the hypothesis of Local Thermodynamic Equilibrium is probably violated (above a few tens of Pa [*Yelle*, 1991]). As for the composition, the mean stratospheric concentrations strongly depend on the top boundary conditions and on the chemistry occurring above, for which we rely on the results of a one-dimensional photochemical model (with no latitudinal nor seasonal variations). The haze production rate is not coupled to the chemistry, although some attempts are under way to include a parameterization of polymerization. Condensation/sublimation of methane, which has been shown to significantly affect the tropospheric circulation [*Tokano et al.*, 2001] is not accounted for. Nor is the possible effect of gravity tides from Saturn [*Tokano and Neubauer*, 2002]. Finally, we had to make an assumption on the thermal inertia of the surface. This thermal inertia was fixed to a low value, typical of continental surfaces on Earth. However, tests done with a much larger thermal inertia, typical of an ocean of water, do not change the results, except slightly in the lower troposphere (results not shown).

[65] Despite all those limitations, the coupled model provides a comprehensive and consistent view of the main observations made by Voyager, and since then by ground-based observations, concerning the composition and dynamics of the stratosphere. In particular, the polar enrichment in chemical compounds in the mid stratosphere caused by downward advection of air coming from the source region [*Lebonnois et al.*, 2001] is remarkably well reproduced with the nominal version of the model. For most species, this polar enrichment has little to do with chemistry. It is due to the contrast between rich air in the polar vortex and uprising clear air having undergone condensation when approaching the tropopause. The amplitude of the polar enrichment is controlled by the competition between vertical advection and latitudinal transport by either the mean meridional wind or parameterized eddies. The modulation of the observed polar enrichment for the various species comes from the different altitudes at which they are removed by condensation and from the altitude of the peak of the observational contribution function. The vertical gradient of atmospheric composition in the polar vortex is also controlled by the balance between vertical advection and latitudinal mixing with the clear air of equatorial latitudes.

[66] Since latitudinal and vertical contrasts are primarily dependent on atmospheric dynamics, it also means that observations of the composition provide a strong constraint on the stratospheric circulation. In particular, the good agreement with available observations for the nominal version provides an indirect but strong validation for the atmospheric regime obtained in the general circulation model (for the mean meridional circulation as well as for the parameterization of latitudinal mixing by waves) and in turn for the explanation put forward for explaining Titan's atmospheric superrotation in previous studies [*Hourdin et al.*, 1995; *Luz et al.*, 2003b].

[67] Note that there is some analogy with the description of humidity contrasts in the Earth's troposphere. For humidity, the source is at the surface and the value at saturation decreases with increasing altitudes up to the tropopause. In the absence of mixing, the specific humidity of a given air parcel corresponds to the smallest humidity at saturation encountered along the parcel trajectory (more or less corresponding to the highest point). There also, water vapor can be used to monitor atmospheric transport and assess transport models [e.g., *Pierrehumbert and Roca*, 1998].

[68] It is not clear yet whether Cassini will be able to monitor cloud motions. It is clear however that the time evolution of stratospheric temperature and composition will provide a strong constraint on the atmospheric dynamics and on the validity of the coupled model which we will continue to develop.

[69] An extended mission beyond the nominal 4 years will probably add a lot to our understanding of the complex machinery of Titan's stratosphere. For instance, the transition period after equinox will bring substantial information on vertical advection in the polar vortex.

[70] **Acknowledgments.** D.L. acknowledges financial support from Fundação para a Ciência e a Tecnologia, Portugal (fellowship PRAXIS XXI/BPD/3630/2000). The graphics have been made with the user friendly and public domain graphical package GrADS originally developed by Brian Doty (COLA, support@grads.iges.org). We also thank the two reviewers, C. P. McKay and I. C. F. Mueller-Wodarg, for their very helpful corrections and suggestions on the first manuscript.

References

Allison, M., D. H. Atkinson, M. K. Bird, and M. G. Tomasko (2004), Titan zonal wind corroboration via the Huygens DISR solar zenith angle measurement, in *Planetary Probe Atmospheric Entry and Descent Trajectory Analysis and Science*, *Eur. Space Agency Spec. Publ.*, *ESA, SP-544*, 125–130.

Bézard, B., A. Coustenis, and C. P. McKay (1995), Titan's stratospheric temperature asymmetry: A radiative origin, *Icarus*, *113*, 267–276.

Bird, M. K., et al. (2002), The Huygens Doppler Wind Experiment—Titan winds derived from probe radio frequency measurements, *Space Sci. Rev.*, *104*, 613–640.

Bouchez, A. H., M. E. Brown, M. Troy, R. S. Burruss, R. G. Dekany, and R. A. West (2003a), Titan's stratospheric zonal winds, paper presented at Division for Planetary Sciences 35th Meeting, Am. Astron. Soc., Washington, D. C.

Bouchez, A. H., M. E. Brown, M. Troy, R. S. Burruss, R. G. Dekany, and R. A. West (2003b), Titan's stratospheric zonal winds, *Bull. Am. Astron. Soc.*, *35*, 928.

Brown, M. E., A. H. Bouchez, and C. A. Griffith (2002), Direct detection of variable tropospheric clouds near Titan's south pole, *Nature*, *420*, 795–797.

Cabane, M., E. Chassefière, and G. Israel (1992), Formation and growth of photochemical aerosols in Titan's atmosphere, *Icarus*, *96*, 176–189.

Coll, P., D. Coscia, S. Smith, M.-C. Gazeau, S. I. Ramirez, G. Cernogora, G. Israël, and F. Raulin (1999), Experimental laboratory simulation of Titan's atmosphere: Aerosols and gas phase, *Planet. Space Sci.*, *47*, 1331–1340.

Coustenis, A., and B. Bézard (1995), Titan's atmosphere from Voyager infrared observations: IV Latitudinal variations of temperature and composition, *Icarus*, *115*, 126–140.

Coustenis, A., B. Bézard, and D. Gautier (1989), Titan's atmosphere from Voyager infrared observations. I. The gas composition of Titan's equatorial region, *Icarus*, *80*, 54–76.

Del Genio, A., and R. J. Suozzo (1987), A comparative study of rapidly rotating dynamical regimes in a terrestrial general circulation model, *J. Atmos. Sci.*, *44*, 973–986.

Del Genio, A. D., W. Zhou, and T. P. Eichler (1993), Equatorial superrotation in a slowly rotating GCM: Implications for Titan and Venus, *Icarus*, *101*, 1–17.

Flasar, F. M. (1998), The composition of Titan's atmosphere: A meteorological perspective, *Planet. Space Sci.*, *46*, 1109–1124.
Flasar, F. M., and B. J. Conrath (1990), Titan's stratospheric temperatures: A case for dynamical inertia?, *Icarus*, *85*, 346–354.
Flasar, F. M., R. E. Samuelson, and B. J. Conrath (1981), Titan's atmosphere: Temperature and dynamics, *Nature*, *292*, 693–698.
Fulchignoni, M., et al. (2002), The characterisation of Titan's atmospheric physical properties by the Huygens Atmospheric Structure Instrument (HASI), *Space Sci. Rev.*, *104*, 395–431.
Gendron, E., et al. (2004), VLT/NACO adaptive optics imaging of Titan, *Astron. Astrophys.*, *417*, L21–L24.
Gibbard, S. G., B. Macintosh, D. Gavel, C. E. Max, I. de Pater, H. G. Roe, A. M. Ghez, E. F. Young, and C. P. McKay (2004), Speckle imaging of Titan at 2 microns: Surface albedo, haze optical depth, and tropospheric clouds 1996–1998, *Icarus*, *169*, 429–439.
Gierasch, P. J. (1975), Meridional circulation and the maintenance of the Venus atmospheric rotation, *J. Atmos. Sci.*, *32*, 1038–1044.
Golitsyn, G. S. (1975), Another look at atmospheric dynamics on Titan and some of its general consequences, *Icarus*, *24*, 70–75.
Griffith, C., T. Owen, G. Miller, and T. Geballe (1998), Transient cloud in Titan's lower atmosphere, *Nature*, *395*, 575–578.
Griffith, C. A., J. L. Hall, and T. R. Geballe (2000), Detection of daily clouds on Titan, *Science*, *290*, 509–513.
Hidayat, T., A. Marten, Y. Biraud, and R. Moreno (2002), Study of the atmosphere of Titan from millimeter and submillimeter observations, in *Proceedings of the IAU 8th Asian-Pacific Regional Meeting*, vol. II, edited by S. Ikeuchi, J. Hearnshaw, and T. Hanawa, pp. 9–10, Astron. Soc. of Jpn., Tokyo.
Hourdin, F., P. Le Van, O. Talagrand, R. Courtin, D. Gautier, and C. McKay (1992), Numerical simulation of the circulation of the atmosphere of Titan, in *Symposium on Titan*, *Eur. Space Agency Spec. Publ.*, *ESA SP-338*, 101–106.
Hourdin, F., O. Talagrand, R. Sadourny, C. Régis, D. Gautier, and C. P. McKay (1995), General circulation of the atmosphere of Titan, *Icarus*, *117*, 358–374.
Hourdin, F., O. Talagrand, K. Menou, R. Fournier, J.-L. Dufresnes, D. Gautier, R. Courtin, B. Bézard, C. P. McKay (1996), Numerical modelling of the circulation of superrotating atmospheres: Venus and Titan, in *Environment Modelling for Space-Based Applications*, edited by A. Hilgers and T.-D. Guyenne, *Eur. Space Agency Spec. Publ.*, *ESA SP-392*, 329–333.
Hubbard, W. B. (1993), The occultation of 28 Sgr by Titan, *Astron. Astrophys.*, *269*, 541–563.
Hunt, B. G. (1979), The influence of the Earth's rotation rate on the general circulation of the atmosphere, *J. Atmos. Sci.*, *36*, 1392–1408.
Hutzell, W. T., C. P. McKay, O. B. Toon, and F. Hourdin (1995), Simulations of Titan's brightness by a two-dimensional haze model, *Icarus*, *119*, 112–129.
Kostiuk, T., K. E. Fast, T. A. Livengood, T. Hewagama, J. J. Goldstein, F. Espenak, and D. Buhl (2001), Direct measurement of winds on Titan, *Geophys. Res. Lett.*, *28*, 2361–2364.
Lebonnois, S., D. Toublanc, F. Hourdin, and P. Rannou (2001), Seasonal variations of Titan's atmospheric composition, *Icarus*, *152*, 384–406.
Lebonnois, S., E. Bakes, and C. P. McKay (2002), Transition from gaseous compounds to aerosols in Titan's atmosphere, *Icarus*, *159*, 505–517.
Lebonnois, S., E. Bakes, and C. P. McKay (2003a), Atomic and molecular hydrogen budget in Titan's atmosphere, *Icarus*, *161*, 474–485.
Lebonnois, S., F. Hourdin, P. Rannou, D. Luz, and D. Toublanc (2003b), Impact of the seasonal variations of composition on the temperature field of Titan's stratosphere, *Icarus*, *163*, 164–174.
Lellouch, E., A. Coustenis, D. Gautier, F. Raulin, N. Dubouloz, and C. Frère (1989), Titan's atmosphere and hypothesized ocean: A reanalysis of Voyager 1 radio-occultation and IRIS 7.7 μm data, *Icarus*, *79*, 328–349.
Lindal, G. F., G. E. Wood, H. B. Hotz, D. N. Sweetnam, V. R. Eshleman, and G. L. Tyler (1983), The atmosphere of Titan: An analysis of the Voyager 1 radio occultation measurements, *Icarus*, *53*, 348–363.
Livengood, T. A., T. Hewagama, T. Kostiuk, K. E. Fast, and J. Goldstein (2002), Improved determination of ethane abundance in Titan's stratosphere, *Icarus*, *157*, 249–253.
Lorenz, R. D., M. T. Lemmon, P. H. Smith, and G. W. Lockwood (1999), Seasonal change on Titan observed with the Hubble Space Telescope WFPC-2, *Icarus*, *142*, 391–401.
Lorenz, R. D., E. F. Young, and M. T. Lemmon (2001), Titan's Smile and Collar: HST observations of seasonal change 1994–2000, *Geophys. Res. Lett.*, *28*, 4453–4456.
Luz, D., and F. Hourdin (2003), Latitudinal transport by barotropic waves in Titan's stratosphere. I. General properties from a horizontal shallow-water model, *Icarus*, *166*, 328–342.
Luz, D., R. Courtin, D. Gautier, J.-P. Lebreton, T. Approuchaux, F. Ferri, L. Lara, A. Kaufer, and F. Hourdin (2003a), Characterization of the zonal wind flow in the stratosphere of Titan with UVES, *Bull. Am. Astron. Soc.*, *35*, 927.
Luz, D., F. Hourdin, P. Rannou, and S. Lebonnois (2003b), Latitudinal transport by barotropic waves in Titan's stratosphere. II. Results from a coupled dynamics-microphysics-photochemistry GCM, *Icarus*, *166*, 343–358.
Marten, A., T. Hidayat, Y. Biraud, and R. Moreno (2002), New millimeter heterodyne observations of Titan: Vertical distributions of nitriles HCN, HC_3N, CH_3CN, and the isotopic ratio $^{15}N/^{14}N$ in its atmosphere, *Icarus*, *158*, 532–544.
McKay, C. P., J. B. Pollack, and R. Courtin (1989), The thermal structure of Titan's atmosphere, *Icarus*, *80*, 23–53.
Moreno, R., and A. Marten (2003), Measurements of zonal winds on Titan from millimeter interferometric observations, *Bull. Am. Astron. Soc.*, *35*, 928.
Pierrehumbert, R. T., and R. Roca (1998), Evidence for control of Atlantic subtropical humidity by large-scale advection, *Geophys. Res. Lett.*, *25*, 4537–4540.
Rannou, P., F. Hourdin, and C. P. McKay (2002), A wind origin for Titan's haze structure, *Nature*, *418*, 853–856.
Rannou, P., F. Hourdin, C. P. McKay, and D. Luz (2004), A coupled dynamics-microphysics model of Titan's atmosphere, *Icarus*, *170*, 443–462.
Raulin, F., and T. Owen (2002), Organic chemistry and exobiology on Titan, *Space Sci. Rev.*, *104*, 377–394.
Roe, H. G., I. de Pater, B. A. Macintosh, S. G. Gibbard, C. E. Max, and C. P. McKay (2002a), NOTE: Titan's atmosphere in late southern spring observed with adaptive optics on the W. M. Keck II 10-meter telescope, *Icarus*, *157*, 254–258.
Roe, H. G., I. de Pater, B. A. Macintosh, and C. P. McKay (2002b), Titan's clouds from Gemini and Keck adaptive optics imaging, *Astrophys. J.*, *581*, 1399–1406.
Roe, H. G., T. K. Greathouse, M. J. Richter, and J. H. Lacy (2003), Propane (C_3H_8) on Titan, *Astrophys. J. Lett.*, *597*, L65–L68.
Rossow, W. B. (1979), Large-scale motion in the Venus stratosphere, *J. Atmos. Sci.*, *36*, 377–389.
Sromovsky, L. A., V. E. Suomi, J. B. Pollack, R. J. Krauss, S. S. Limaye, T. Owen, H. E. Revercomb, and C. Sagan (1981), Implications of Titan's north-south brightness asymmetry, *Nature*, *292*, 698–702.
Tokano, T., and F. M. Neubauer (2002), Tidal winds on Titan caused by Saturn, *Icarus*, *158*, 499–515.
Tokano, T., F. M. Neubauer, M. Laube, and C. P. McKay (2001), Three-dimensional modeling of the tropospheric methane cycle on Titan, *Icarus*, *153*, 130–147.
Toon, O. B., C. P. McKay, T. P. Ackerman, and K. Santhanam (1989), Rapid calculation of radiative heating rates and photodissociation rates in inhomogeneous multiple scattering atmospheres, *J. Geophys. Res.*, *94*, 16,287–16,301.
Tran, B. N., J. P. Ferris, and J. J. Chera (2003), The photochemical formation of a Titan haze analog: Structural analysis by X-ray photoelectron and infrared spectroscopy, *Icarus*, *162*, 114–124.
Wilson, E. H., and S. K. Atreya (2003), Chemical sources of haze formation in Titan's atmosphere, *Planet. Space Sci.*, *51*(14–15), 1017–1033.
Yelle, R. V. (1991), Non-LTE models of Titan's upper atmosphere, *Astrophys. J.*, *383*, 380–400.
Yelle, R. V., J. I. Lunine, and D. M. Hunten (1991), Energy balance and plume dynamics in Triton's lower atmosphere, *Icarus*, *89*, 347–358.
Young, E. F., P. Rannou, C. P. McKay, C. A. Griffith, and K. Noll (2002), A three-dimensional map of Titan's tropospheric haze distribution based on Hubble Space Telescope imaging, *Astron. J.*, *123*, 3473–3486.

F. Hourdin and S. Lebonnois, Laboratoire de Météorologie Dynamique, IPSL, CNRS/UPMC, Box 99, F-75252 Paris Cedex 05, France. (frederic.hourdin@lmd.jussieu.fr; sllmd@puente.lmd.jussieu.fr)

D. Luz, LESIA, Observatory of Paris, Meudon, France and Centro de Astronomia e Astrofísica da Universidade de Lisboa, Lisbon, Portugal. (david.luz@obspm.fr)

P. Rannou, Service d'Aéronomie, Institut Pierre-Simon Laplace, Paris, France. (pra@ccr.jussieu.fr)